Proceedings of the ASME 2010 3rd Joint US-European Fluids Engineering Summer Meeting and 8th International Conference on Nanochannels, Microchannels, and Minichannels
FEDSM-ICNMM2010
August 1-5, 2010, Montreal, Canada

FEDSM-ICNMM2010-30997

Internal Turbulent Flow Induced Pipe Vibrations with and without Baffle Plates

Andrew S. Thompson, Daniel Maynes, Jonathan D. Blotter
Department of Mechanical Engineering
Brigham Young University
Provo, UT, USA

ABSTRACT

The induced vibration in pipes due to turbulent flow through them is important in many industries and applications. This paper presents the results of an experimental investigation that characterizes pipe wall vibration caused by turbulent internal flow. Experiments were conducted using a water flow loop to characterize how the pipe wall vibration depends on the average flow speed, the pipe diameter, and the pipe thickness for fully-developed turbulent pipe flow. Experiments were also conducted to characterize the influence on the pipe response of turbulence generation due to the flow passing through baffle plates with various hole sizes and constant through area. All experiments were conducted using PVC pipe with diameters ranging from 51 mm to 102 mm and diameter to thickness ratios ranging from 8.9 to 16.9. Average flow speeds for the experiments ranged from 3 to 11.5 m/s and the baffle plates employed exhibited hole sizes ranging from 1.6 to 25 mm. Accelerometers mounted on the pipe walls were used to characterize the pipe vibrations. The results show that for fully developed turbulent flow the rms of the pipe wall acceleration scales nominally as the square of the average fluid speed and increases with decreasing pipe wall thickness. Based on the data, a non-dimensional parameter describing the pipe wall acceleration for the fully-developed turbulent flow scenario is proposed and its dependence on relevant independent nondimensional parameters is presented. Lastly, when turbulence was induced using baffle plates the localized turbulence intensity was greatly increased. For the largest holed baffle plates, cavitation was observed to occur, significantly increasing the rms pipe wall acceleration. As baffle plate hole size decreased, vibration levels were observed to approach levels that were measured when no baffle plate was employed. For all baffle plate experiments the magnitude of the vibration was observed to decrease with increasing downstream distance from the turbulence source, approaching the baseline no baffle plate case.

1. INTRODUCTION

The conveyance of fluids through pipes is an integral part of world-wide economic activity and has contributed to the progress that has occurred over the last century. These pipes are prone to cyclic loading, in the form of pipe vibrations, induced by internal turbulent flow. Vibration loading becomes a problem as piping infrastructure ages, contributing to fatigue induced failure. For instance, in the U.S. about 60% of the pipelines have been in use for over 25 years and are becoming prone to failure [1]. This may lead to economic loss as well as environmental and societal damage. Therefore the characterization of turbulence induced pipe vibrations is important in many industries and applications.

For example, related work with relevance to the nuclear power industry, explored external turbulent flow past cylindrical rods. This work showed that rod vibrations are due to turbulent pressure fluctuations in the boundary layer. It was also shown that the vibration levels are proportional to the average fluid velocity squared[2]. Several researchers have proposed correlations between the vibration level, in terms of the characteristic amplitudes of displacement or acceleration, and the fluid dynamic and geometric parameters[3-5]. These dependent variables include the average fluid speed, the rod diameter, the fluid density, the mass per unit length of the rod, etc.

Concerning fully developed turbulent pipe flow several research groups, using both experimental and numerical approaches, have shown that pipe vibration levels increase with increasing flow dynamic pressure [6-11]. Although results from each investigation have shown differences, each study has concluded that the pipe vibration is a direct result of the inherent spatially and temporally varying pressure at the pipe wall. It is well known that the flow field is made up of eddies of various sizes. The turbulent kinetic energy of these eddies is transferred from large eddies into smaller eddies. As these eddies approach the pipe wall, most of their energy is converted into pressure fluctuations which induce pipe vibrations [4, 6, 12].

Large amplitude vibrations have also been observed in piping systems in French nuclear power plants, as flows passed through single hole orifices. Experiments to determine the cause of these unwanted vibrations concluded that they were caused by supercavitation at the orifice[13]. This cavitation induced vibration can be identified by computing the power spectral density of wall mounted acceleration measurements. Specifically, cavitation adds a broad increase to the spectrum with an amplitude that depends on the incipient cavitation[14]. Because piping systems incorporate other components, such as orifices or valves, it may be important to identify how they affect the vibrational response of the system.

Although excessive vibrations can lead to unwanted consequences, the monitoring of vibration levels can also be implemented to provide non-intrusive flow sensing. Most flow sensors in use today require interrupting the flow, which, for some applications, is not always feasible. A non-intrusive technique has been proposed by several researchers and has broad application throughout industry[4,10,12]. There is thus a clear need to understand how the vibration levels depend on both the flow dynamics and the pipe characteristics. In general these include: average fluid speed, fluid density, turbulence levels, pipe diameter, pipe wall thickness, pipe length, pipe material, etc.

The focus of this paper is to present results of an experimental investigation that uses wall mounted accelerometers to characterize pipe wall vibration due to internal, fully-developed turbulent pipe flow. From the accelerometer measurements, the influence of the average fluid speed, the pipe diameter, and the pipe wall thickness on the pipe vibration are all explored. For all results presented here the pipe was hung supported with flexible cables. Specifically, experiments were conducted in PVC test sections of internal diameters of 51 mm – 101.6 mm, and pipe wall diameter to thickness ratios ranging from 8.9 – 16.9. The experiments were conducted with average fluid speeds ranging from 0 – 11.5 m/s. Further, data published previously[6] are also examined to characterize the influence of pipe material on vibration levels. This previous work studied the relationship between pipe vibration and pipe flow in aluminum, stainless steel and PVC pipes.

Also presented are results characterizing the influence of baffle plates of varying hole size on the vibration levels. Baffle plate hole size varied between 1.6 to 25 mm. Wall mounted acceleration measurements were taken at various streamwise distances downstream from the from the baffle plates in each PVC test section.

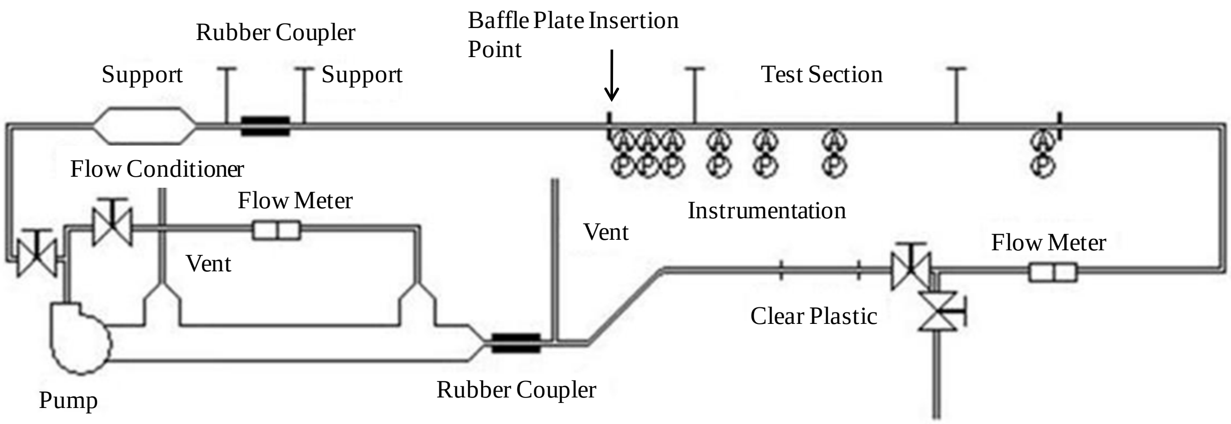

Figure 1: Schematic illustration of the BYU water loop used for experiments.

2. METHODOLOGY

2.1 Water Flow Loop

Experiments were conducted in a water flow loop facility at Brigham Young University (BYU). A schematic illustration of the flow loop is shown in Fig. 1. Water was circulated via a Bell and Gossett 75 hp, 1800 RPM centrifugal pump driven by a 75 hp Marathon Electric 365T motor. Water was used as the working fluid and the loop was filled by two open vertical vent columns. These vents extend above the level of the rest of the system and keep the flow loop slightly pressurized to keep air from leaking in. The vertical columns also serve to vent air bubbles that develop during the filling process and to maintain nearly atmospheric pressure at the pump inlet. The pump inlet is fed by 203.2 mm schedule 80 PVC pipe. The pump outlets to 101.6 mm schedule 80 pipe, which divides into bypass and main branches. Each branch is controlled by a hand-actuated valve, allowing the flow through each section to be controlled. The bypass line provided a way to control flow rate without changing pump speed.

The main line expands to 203.2 mm schedule 80 PVC to accommodate a flow conditioner to minimize the influence of pump induced vibration. The flow conditioner was constructed from 76.2 mm thick aluminum honeycomb and several layers of polyethylene mesh to facilitate dissipation of coherent turbulent structures and swirl induced by the pump. After the flow conditioner, the pipe contracts to 101.6 mm schedule 80 pipe. After the contraction, the outlet is connected to a flexible rubber coupler. The coupler reduces structural vibrations transmitted to the test section from the pump and pipe components and is connected to the building wall by two wall mounts (one up-stream and one down-stream) to absorb low frequency pipe swaying. The flow is then allowed to develop over 6.096 m of pipe (L/D > 60). The water then passes into the test section, which is described in further detail in section 2.2. After the test section, the flow passes through another 6.096 m section after which it is returned to the pump. On the return portion of the flow loop, a clear section of schedule 40 PVC is mounted in line to allow visual inspection of the flow.

2.2 Test Sections and Instrumentation

The test sections consist of 6.096 m interchangeable sections of 50.8 mm, 76.2 mm, and 101.6 mm diameter schedule 40 and 80 PVC pipe (see Figure 2) hung supported by ceiling mounts. The actual pipe diameters, *D*, and wall thicknesses, *t*, are shown in Table 1.

Table 1: Internal pipe diameters and wall thicknesses for experiments with PVC pipes.

Pipe Schedule	*D* (m)	*t* (m)	*D/t*
50.8 mm Sch 80	0.049	0.0055	8.899
76.2 mm Sch 80	0.074	0.0076	9.672
101.6 mm Sch 80	0.097	0.0086	11.355
50.8 mm Sch 40	0.053	0.0039	13.427
76.2 mm Sch 40	0.078	0.0055	14.215
101.6 mm Sch 40	0.102	0.0060	16.944

PCB 352B68 accelerometers with nominal sensitivities of 10.2 mV/g were used to measure the pipe wall acceleration. Accelerometers were placed on opposite sides of the test section at six discrete axial locations. A fluctuating pressure transducer (PCB 102A02S) with a nominal sensitivity of 7.3 mV/kPa was also placed on the side of the test section. The pressure transducer was located at the same axial locations as the accelerometers. On the return leg of the flow loop, two Omega FP6500 paddle wheel flow meters with a range of 0.1-12 m/s and an accuracy of ±1.5% were used to measure the average velocity of the water through the

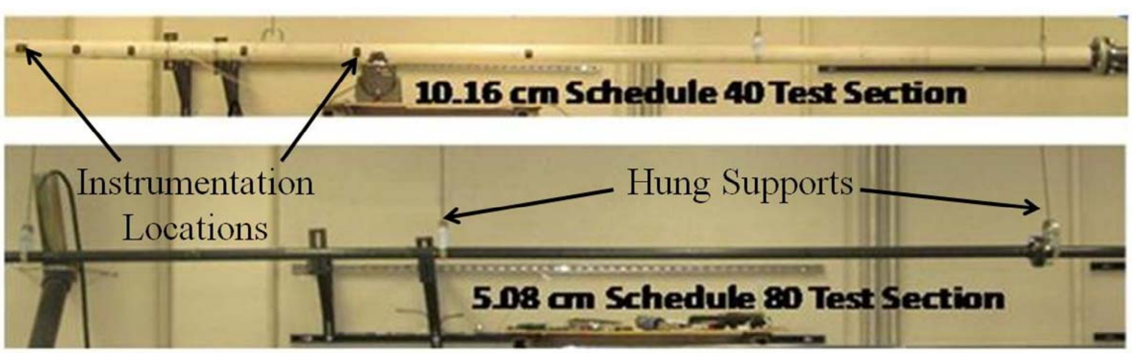

Figure 2: Photograph of 101.6 mm and 50.8 mm test sections.

pipe. The total pressure drop across the length of the test section was also measured. As noted previously, the present results are also compared to data obtained and reported on previously by Pittard *et al.*[11] where three different pipe materials were employed. The pipe characteristics for the results of Pittard *et al.* are shown in Table 2.

Table 2: Pipe material, diameters, and wall thicknesses for data of Pittard, et al [11].

Pipe Schedule	Material	*D* (m)	*t* (m)
101.6 mm Sch 40	PVC	0.102	0.00602
76.2 mm Sch 40	PVC	0.0779	0.00548
76.2 mm Sch 40	Aluminum	0.0779	0.00548
76.2 mm Sch 40	Stainless Steel	0.0779	0.00548
38.1 mm Sch 40	Stainless Steel	0.041	0.00368

2.3 Baffle Plates

In order to produce various levels of turbulence in the test sections, holed baffle plates were inserted between the flanges that connected the end of the developing region and the test sections, with the holes parallel to the pipe axis. Five baffle plates were machined from 6.35 mm thick aluminum plate with 25.4 mm, 12.7 mm, 6.35 mm, 3.18 mm, and 1.59 mm holes drilled into them. The center pitch of the holes (distance between the center of one hole and the center of the next hole) was 32 mm, 16 mm, 8 mm, 4 mm, and 2 mm respectively. The through area of the holes in each baffle plate was constant and equal to 3548 mm^2. This results in seven holes for the 25.4 mm baffle plate and 1793 holes for the 1.59 mm baffle plate.

2.4 Data Acquisition

A PC based data acquisition system consisting of a multi channel National Instruments data acquisition module was used to collect acceleration, flow rate, and fluctuating pressure time series data. For the accelerometer and pressure fluctuation time series data the rms values of the time series were computed. These values are referred to here as A' and P' respectively, and represent typical magnitudes in the pipe wall acceleration and internal surface pressure fluctuations. The accelerometer data were also integrated to yield pipe velocity (integrated once). Subsequently the rms value of the pipe velocity, V', was also computed. However, the results presented in this paper will focus on A'. All of the sensors were sampled for 10 second intervals at a sample rate of 5000 Hz.

Experiments were conducted in the following manner. For each test section, the pump was set at a desired speed and the flow was allowed to become steady. Then 10 seconds of time series data were acquired at 5000 Hz. The pump speed was then adjusted and the process repeated to acquire 24-29 discrete flow speeds. Subsequently, the baffle plates were inserted and experiments were repeated in the same fashion.

2.5 Pump Effects

Accelerometers were mounted directly on the pump to characterize the spectral content of the pump vibration. In general the dominant vibration frequencies were relatively low, with the exception of a spike at the impeller rotation frequency. This spike did not appear in the frequency spectrum of the accelerometer measurements on the pipe test section.

Although not attributed to the pump, low frequency drift in the accelerometer measurements was observed at low and no flow. Therefore, these data were filtered with a high pass filter of 2 Hz. Thus, except at flow rates lower than presented in this paper the influence of the pump on the acquired data is minimal.

3. RESULTS

3.1 Wall pressure Fluctuations

The rms of the pressure fluctuations, P', as a function of the average fluid speed for the six test sections listed in Table 1 was measured and is shown in Fig 3. At low speeds some scatter exists in the data due to resolution limits of the sensors. At higher speeds however, ($V_f > 2$ m/s) the trend in the data is similar for all test sections. Namely, the P' vs. V_f trend exhibits a power law relation, $P' \sim V_f^m$. A least squares fit to each data set shown in Fig. 3 over the range $V_f > 2.5$ m/s reveals that m varies from 1.91 to 2.07 with an average value of 2.02. There appears to be no systematic variation in m. This result shows that P' scales directly with the average fluid dynamic pressure (ρV_f^2).

When plotted as a function of V_f, the P' data for the 10.16 cm diameter schedule 40 test section shows the largest magnitude at a given V_f. The magnitude of the P' data 101.6 mm test sections appears to be larger than the data for the 76.2 mm test sections, which are larger than the data for the 50.8 mm test sections. As expected, however, there seems to be no systematic variation in *P'* with diameter to thickness ratio (*D/t*).

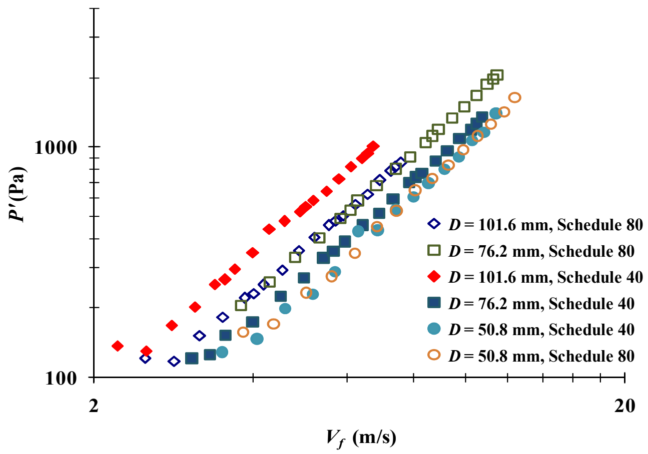

Figure 3: P' as a function of the average fluid speed, V_f for flow through the six test sections.

3.2 Accelerometer Measurements

Figure 4 shows *A'* as a function of V_f along the length of the 101.6 mm schedule 40 test section, where *x/D* represents the ratio of the distance from the test section entrance to inner pipe diameter. Data are shown at *x/D* = 3, 6, 9, 15, 21, 30, and 57. Like the pressure fluctuation measurements, these data exhibit a power law behavior of the form $A' \sim V_f^n$. Above a flow speed of 3.5 m/s, *n* varies from 1.91 to 2.39 for the various *x/D* locations, with an average value of 2.14. The data displayed in this figure exhibit very little variation in *A'* with *x/D*. Similar behavior is observed for the other test sections explored. Because of this, *A'* for each test section is averaged over all *x/D* locations.

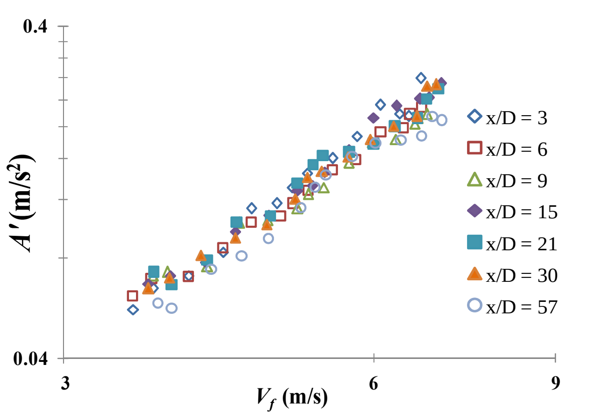

Figure 4: A' as a function of V_f at seven x/D locations along the length of the 101.6 mm schedule 40 test section.

Figure 5 shows *A'* vs. V_f for each of the test sections considered. Again, these data exhibit a power law relationship of the form $A' \sim V_f^m$, where *m* varies from 1.94 to 2.19, with an average value of 2.06.

Modest variation between schedule 40 and 80 data sets exist for each pipe diameter, with the general trend being an increase in $A'$with decreasing schedule size.

The wall thickness for the schedule 80 test sections is about 40% greater than for the schedule 40 test sections while the diameters differ from 3-6%, respectively. Figure 6 presents A' as a function of pipe diameter to thickness ratio, *D/t*, for each test section considered, at a constant fluid velocity of 6.7 m/s. Although there are only two points for each pipe diameter, the trend clearly shows that A'increases with increasing *D/t*.

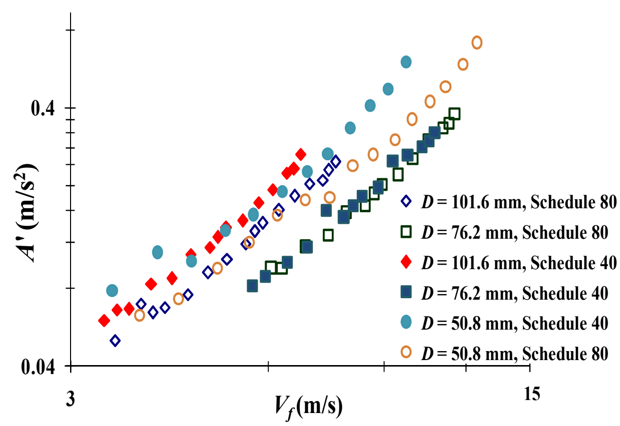

Figure 5: A' as a function of V_f for flow through the six test sections considered.

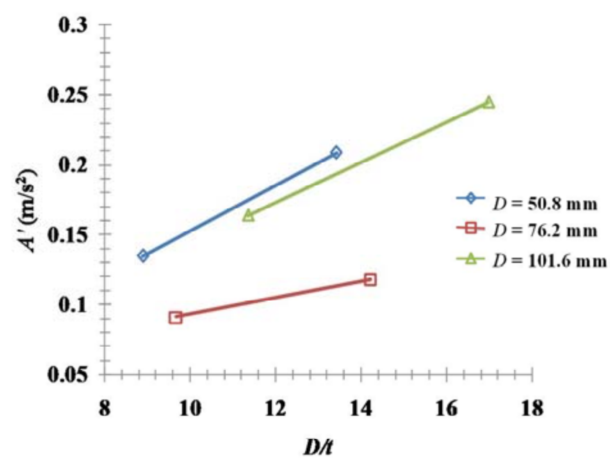

Figure 6: A' as a function of D/t at $V_f \approx 6.7$ m/s for each the three diameter pipes considered.

3.3 Dimensionless A'

It has been shown above that *A'* scales nominally as V_f^2 and *D/t*. In general, the rms of the pipe wall acceleration can be written as a function of all the variables that exert influence:

$$A' = f\left(V_f, D, t, \rho, \mu, \rho_{eq}\right) \qquad (3)$$

where ρ_{eq} is the equivalent density, which accounts for the combined mass of the pipe and the fluid. [15]

$$\rho_{eq} = \frac{\rho\pi\left(\frac{D}{2}\right)^2 + \rho_p 2\pi\left(\frac{D}{2}+\frac{t}{2}\right)t}{2\pi t\left(\frac{D}{2}+\frac{t}{2}\right)} \qquad (4)$$

Recasting this set of dimensional variables into dimensionless form following the standard approach yields the following set of dimensionless variables.

$$A^* = \frac{A' t}{V_f^2} \qquad (5)$$

$$Re = \frac{\rho V_f D}{\mu} \qquad (6)$$

$$t^* = \frac{t}{D} \qquad (7)$$

$$\rho^* = \frac{\rho_{eq}}{\rho} \qquad (8)$$

The dimensionless pipe acceleration can then be expressed as a function of the dimensionless variables listed in Eqs. 6 to 8:

$$A^* = f(Re, t^*, \rho^*) \qquad (9)$$

In a parallel numerical investigation using a Large Eddy simulation approach of this same phenomena, Shurtz observed that the A^* normalization is the appropriate dimensionless of *A'* [15]. By holding all but one of the dimensionless variables listed in Eqs. 6 to 8 constant, Shurtz [15] was able to determine the first order effects of each of the dimensionless variables on A^*. These results are listed in Table 3 as power law fits of the data ($A^* \sim Z^{*m}$) that were obtained using the numerical model, where $Z^*$is one of the dimensionless variables listed in Eqs. 6 to 8. The table shows that all of the dimensionless variables, except ρ^*, have a very weak influence on A^*. In the present experiments it is impossible to hold all but one of the pipe dimensionless independent parameters constant. However, it is still useful to explore how A^* depends on each parameter.

Table 4 lists the values of *m* corresponding to $A^* \sim Re^m$ power law fits to the present experimental data for each of the six test sections considered. There appears to be no systematic pattern in the variation of the values of *m* among the test sections and the average value of *m* suggests a very weak dependence of A^* on *Re*. The dependence of A^* on *Re* is slightly different than that observed in the numerical simulations of Shurtz [15]. This is likely due to the fact that Shurtz considered a hydraulically smooth pipe and the results of the present experiments show that the pipes employed exhibit behavior more characteristic of rough pipes where the influence of *Re* is less pronounced.

The present data also show that the dimensionless pipe wall vibration, A^*, is a weak function of t^* following the general pattern shown by the numerical results of Shurtz [15].

The results of the numerical investigation of Shurtz suggests that to a first order the pipe wall vibrations should scale as $A' \sim V_f^2/t^*\rho^*$ for an unsupported pipe [15].

Table 3: The values of *m* corresponding to $A^* \sim Z^{*m}$ power law fit determined by a numerical simulation of flow induced pipe vibrations presented by Shurtz[15].

	m
Re	-0.18
t^*	0.04
ρ^*	-1.00

Table 4: The values of *m* corresponding to $A^* \sim Re^m$ power law fit for each of the six test sections considered.

Test Section	***m***
101.6 mm, Sch 40	0.012
101.6 mm, Sch 80	0.137
76.2 mm, Sch 40	-0.09
76.2 mm, Sch 80	0.015
50.8 mm, Sch 40	-0.11
50.8 mm, Sch 80	-0.07
Average	-0.018

Shown in Fig. 7 is *A'* as a function of $V_f^2/t^*\rho^*$ for each of the six unsupported test sections considered. This figure also includes power law fits of the data with a zero intercept that pass through the schedule 40 and 80 test section data for each pipe diameter (101.6 mm, 76.2 mm, and 50.8 mm). This functional relationship causes the data from the 101.6 mm and 50.8 mm test sections to collapse to nominally a single curve. The 76.2 mm schedule 40 and 80 data also collapse onto each other, however, the magnitude of this collapsed data is smaller than for the 101.6 mm and 50.8 mm data. Much of the behavior in *A'* appears to be captured by the parameter $V_f^2/t^*\rho^*$. It should be noted however, that holding one dimensionless variable constant while changing the others was not possible for these experimental measurements, thereby introducing confounding influences.

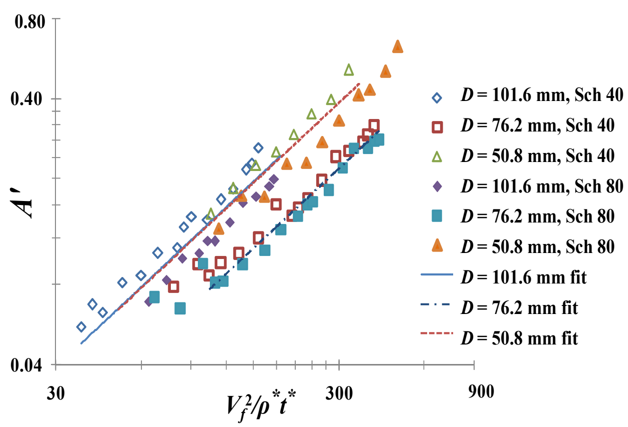

Figure 7: *A'* vs. V_f^2/ρ^*t^* for each of the six test sections considered. Power law fit lines with zero intercept pass through the schedule 40 and 80 pipe section data for each diameter test section.

Figure 8 shows *A'* as a function of $V_f^2/t^*\rho^*$ for the data presented by Pittard *et al.* [11]. The pipe properties for this work are listed in Table 2. This functional relationship causes *A'* for each pipe material and diameter (except for the 38.1 mm stainless steel test section) to collapse onto one another. What is interesting to note is that although these data were collected from a different facility and the pipe moduli and densities vary greatly, the functional relationship, $A' \sim V_f^2/t^*\rho^*$, works quite well to collapse most of these data as well.

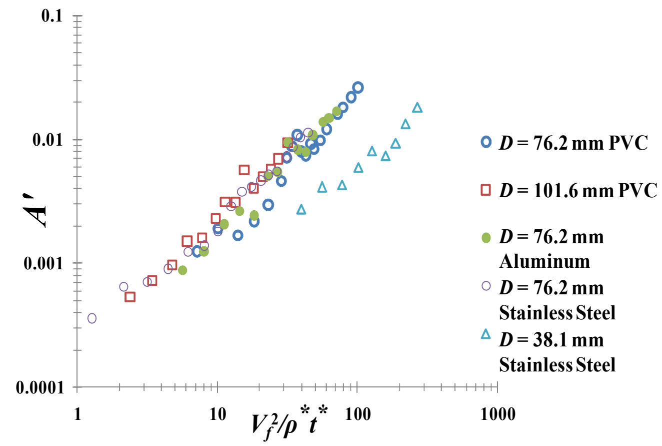

Figure 8: *A'* vs. V_f^2/ρ^*t^* for the data presented by Pittard *et al.* [11].

3.4 Baffle Plate Influence

As discussed in section 2.3 baffle plates were inserted at the test section entrance as turbulence inducers. Five plates were used, each with a different diameter and number of holes drilled into them. The diameters of the holes were 25.4 mm, 12.7 mm, 6.35 mm, 3.18 mm, and 1.59 mm, with the hole diameter being how each baffle plate is distinguished in this paper. The plates were fabricated so that the through area of the holes was 3548 mm^2, resulting in various numbers of holes in each plate (*e.g.* seven holes for the 25.4 mm plate, 28 holes for the 12.7 mm baffle plate, 112 holes for the 6.35 mm baffle plate, 448 holes for the 3.18 mm baffle plate, and 1793 holes for the 1.59 mm plate). The 101.6 mm schedule 40 test section was the only test section used for the baffle plate experiments.

Figure 9 illustrates the influence of each baffle plate on *A'* at seven flow velocities 0.305 m downstream from the baffle plate. The data are plotted versus the ratio of the baffle plate thickness to hole diameter.

The data of Fig. 9 show that the 25.4 mm and 12.7 mm baffle plates (t_{baffle}/D_{hole} = 0.25 and 0.5 respectively) result in the largest increases in the magnitude of *A'*; although for all baffle plates the pipe acceleration increases. The largest increases prevail when cavitation occurs. Cavitation existed for the largest baffle plates and was accompanied by audible noise. Evidence of cavitation in these data is shown in Fig. 8 between a flow speed of 3.07 m/s and 3.72 m/s with the 25.4 mm baffle plate. At this V_f the magnitude of *A'* suddenly jumps. Although not as apparent, cavitation appears to occur between 3.07 m/s and 3.97 m/s in the 12.7 mm baffle plate. What is also evident is that as t_{baffle}/D_{hole} increases, the magnitude of *A'* decreases;

apparently due to an upward shift in the velocity at which cavitation occurs and a reduction in the size of turbulent eddies formed.

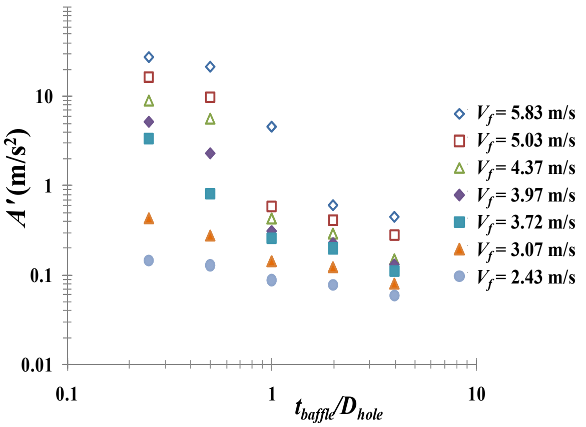

Figure 9: A' as a function of t_{baffle}/D_{hole} for various flow velocities in the 101.6 mm schedule 40 test section 0.305 m from each of the five baffle plates.

Figure 10 presents A' as a function of V_f at various x/D locations along the test section for the 25.4 mm baffle plate. Also shown are data for the no baffle plate scenario. As previously stated, cavitation is occurring at the baffle plate holes, for this plate, and its effect on A' propagates down the entire length of the test section. Cavitation appears to be initiated at a fluid speed of about 3 m/s causing A' to rise rapidly with increasing V_f. At a flow speed of nominally 4 m/s, the rate of increase in A' levels off and becomes similar at all x/D. The magnitude of A' decreases with increasing x/D and decreases towards the vibration levels of the no baffle plate scenario at large x/D. A power law curve fit ($A' \sim V_f^m$) to the data above a flow speed of 4 m/s results in values of the power, m, ranging from 4.12 to 3.36 for the various x/D positions and is included in Table 5. At x/D = 3 and a flow speed of nominally 5.5 m/s, A' is observed to be about 300 times greater than for the no baffle plate case and at x/D = 57 (end of the test section), A' is nominally 20 times greater.

Figures 11 and 12 show A' as a function of V_f for the 6.35 mm baffle plate (t_{baffle}/D_{hole}=1.0) and 1.59 mm baffle plate (t_{baffle}/D_{hole}=4.0), respectively. In Fig. 11, cavitation appears to be initiating only at the highest flow speed. Further, the magnitude of A' is significantly lower than what was shown for the 25.4 mm baffle plate data in Fig. 9. At a flow speed of nominally 5.5 m/s, A' is only about 20 times greater than for the no baffle plate case at x/D = 3. A power law fit of the data with the exponents included in Table 5, show that as x/D increases the value of m approaches the no baffle plate case. This becomes even more apparent for the 1.59 mm baffle plate (Fig. 12). Here the magnitude of A' at x/D = 3 is only about two times greater than for the no baffle plate case. The value of m also changes very little with x/D, with an average value of 2.04. These values are also included in Table 5. There appears to be little systematic variation in the value of m with x/D for the 1.59 mm baffle plate scenario. However, for the 6.35 mm baffle plate scenario, the value of m decreases with increasing x/D. The values of m appear to exhibit the same behavior for the 25.4 mm baffle plate except at the end of the test section, where the values of m begin to increase again. Comparing the values of m for the three baffle plate scenarios presented in Table 5 the general trend is that m increases with increasing baffle plate hole diameter.

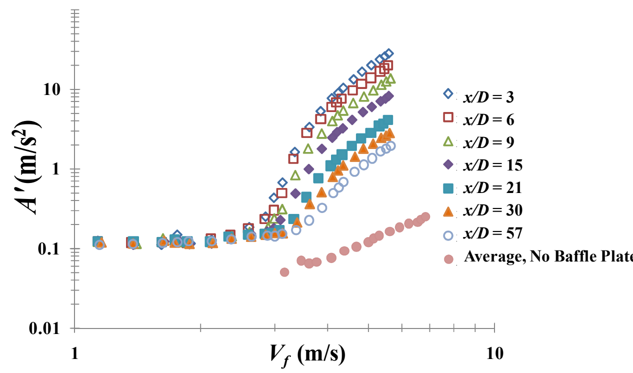

Figure 10: A' vs. V_f at seven x/D locations along the test section length with the 25.4 mm baffle plate. A' for the test section with no baffle plate has been included for reference.

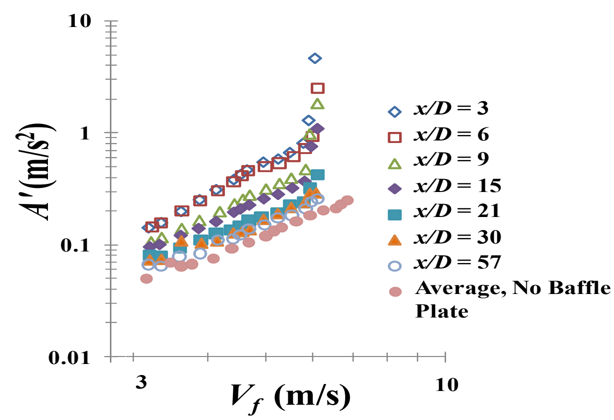

Figure 11: A' vs. V_f at seven x/D locations along the test section length with the 6.35 mm baffle plate. A' for the test section with no baffle plate has been included for reference.

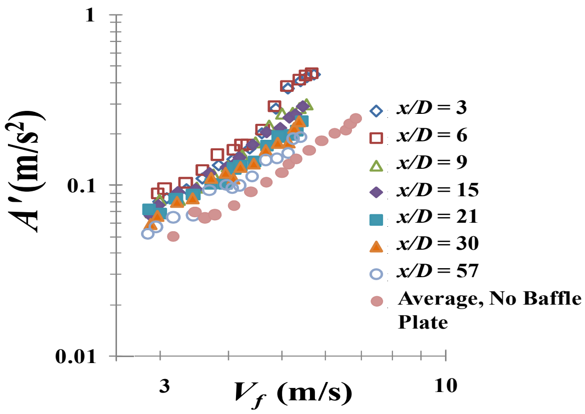

Figure 12: A' vs. V_f at seven x/D locations along the test section length with the 1.59 mm baffle plate.

Figure 13 illustrates how the magnitude of *A'* decays with *x/D* for each baffle plate case at a constant flow speed of 3.61 m/s. As expected, the magnitude of *A'* for the no baffle plate case is nominally flat along the test section length. Although the flow velocity is relatively low, cavitation is occurring with the 25.4 mm and 12.7 mm baffle plates. For these cases, the decay in the magnitude of *A'* appears to be steeper than for the three other scenarios. The test section may not be long enough for *A'* to return to the baseline levels characteristic of the no baffle plate case. The magnitude of *A'* for the 3.18 mm and 1.59 mm baffle plates has decayed to the no baffle plate values by nominally *x/D* = 9. For the 6.35 mm baffle plate *A'* decays to the baseline value at *x/D* = 15.

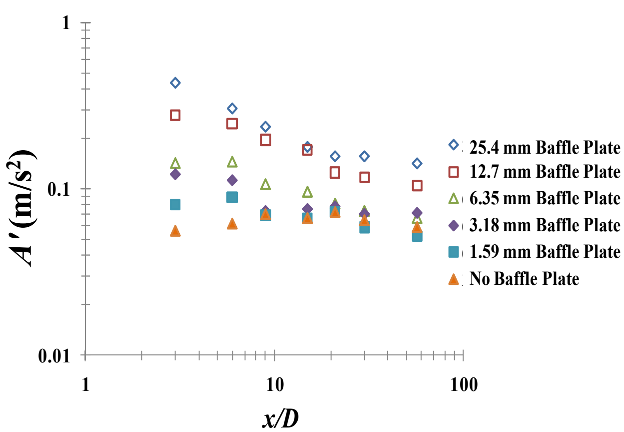

Figure 13: The decay of A' with x/D for each baffle plate case at a flow speed of 3.61 m/s.

As the flow speed increases to 6.84 m/s, as illustrated by the results of Figure 14, it is evident that the decay in the magnitude of *A'* is pushed further downstream. In the cases where cavitation is occurring, the magnitude of *A'* doesn't begin to level off until above *x/D* = 30. The magnitude of *A'* with the 3.18 mm and 1.59 mm baffle plate has decayed to the no baffle plate levels by *x/D* = 15, and by *x/D* = 30 for the 6.35 mm baffle plate.

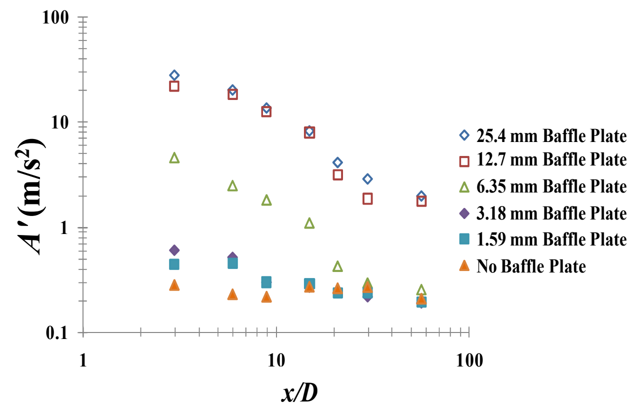

Figure 14: The decay of A' with x/D for each baffle plate case at a flow speed of 6.84 m/s.

These figures indicate that *A'* decays with increasing distance from the baffle plate. At *x/D* = 30, this streamwise position is nearly far enough away from the baffle plates for the flow to be considered fully developed again. The implication is that sufficiently far away from a turbulence source that is not inducing cavitation, the magnitude of *A'* approaches a condition representative of the baseline fully-developed turbulent pipe flow.

Table 5: The value of m from a power law fit of the 25.4 mm, 6.35 mm, and 1.59 mm baffle plate data with x/D.

	Baffle Plate Hole Size			
x/D	**25.4mm**	**6.35 mm**	**1.59 mm**	**No Plate**
3	4.12	2.93	2.02	
6	3.78	2.75	1.92	
9	3.54	2.45	2.29	
15	3.36	2.28	2.19	2.03
21	3.70	2.03	1.89	
30	3.47	1.95	2.00	
57	3.85	2.09	1.98	
Average	3.69	2.35	2.04	

4. CONCLUSIONS

This paper presented the results of an experimental investigation to characterize pipe vibrations induced by turbulent pipe flow. Experiments were conducted using a water flow loop to address two general phenomena related to pipe vibration: 1) How the pipe vibration depends on the average flow speed, pipe diameter, and pipe thickness. 2) How turbulence generation caused by holed baffle plates influence the pipe response.

When comparing a power law fit of the average of *P'* along the pipe length to V_f, it was found that *P'* scaled nearly as V_f^2, with the power from the experimental data varying less than 5% from an expected value of 2.0. It was determined that *A'* for each of the test sections also scaled nearly quadratically with V_f, with an average power of 2.06 over all the test sections. Put differently, *P'* and *A'* are proportional to the dynamic pressure in the pipe.

When comparing the dimensionless pipe wall acceleration (A^*) to the dimensionless parameters *Re*, t^*, and ρ^*, it was found that A^* was weakly dependent on all of them except ρ^*. This was in good agreement to a parallel numerical study performed by Shurtz [24]. This strong dependence on ρ^* resulted in the scaling relationship, $A' \sim V_f^2/t^*\rho^*$. It was found that this expression collapses *A'* data for PVC, steel and aluminum pipes. However, use of this expression for pipe diameters and wall thicknesses deviating significantly than those used in the present experiments is not recommended. This scaling relationship is a first order estimate of the expected level of pipe vibration in a long pipe. Further studies are currently ongoing that will examine the effects of diameter, wall thickness, and fluid density. While the pipe modulus does not appear in this scaling expression, recent numerical work has also shown that with regard to pipe wall acceleration in long pipes that the pipe modulus exercises only modest influence and its influence is easily masked by varying pipe density, which is included in the scaling expression[15].

It was found that placing baffle plates into the flow would induce turbulence downstream of the baffle plate. For large baffle plate hole sizes cavitation existed at high fluid speeds. Cavitation would cause the magnitude of *A'* to increase by up to 300 times. As the baffle plate hole size decreased, it was observed that the fluid speed at which cavitation would initiate would increase. Cavitation was not prevalent at all with baffle plate hole sizes smaller than 6.35 mm. Further, it was observed that as the baffle plate hole size decreased, *A'* would approach magnitudes shown with the no baffle plate baseline. *A'* was also observed to decay to baseline levels as the distance from a non-cavitating baffle plate increased.

NOMENCLATURE

A^* : Dimensionless pipe acceleration.
A' : Rms of the time series acceleration signal.
D : Pipe diameter.
D_{hole} : Baffle plate hole diameter.
P' : Rms of the time series pressure signal.
Re : Reynold's number.
V_f : Fluid velocity.
Z^* : A generalized dimensionless variable.
m : Power law curve fit exponent.
n : Power law curve fit exponent.
t^* : Dimensionless pipe thickness.
t : Pipe thickness.
t_{baffle} : Baffle plate thickness.
x : Axial pipe distance.
ρ^* : Dimensionless pipe/fluid density.
ρ : Fluid density.
ρ_{eq} : Equivalent density of the fluid and pipe material.
ρ_p : Pipe material density.

ACKNOWLEDGEMENTS

The authors acknowledge CCI Control Components Inc. and Genscape Inc. for their generous support of this work.

REFERENCES

1. Awawdeh, A., Bukkapatnam, S.T.S., Kumara, S.R.T., *et al.*, "Wireless sensing of Flow-Induced Vibrations for Pipeline Integrity Monitoring," *IEEE SAM 06*, Boston, July 2006.
2. Paidoussis, M.P., "Fluidelastic Vibratio of Cylinder Arrays in Axial and Cross Flow: State of the Art," *Journal of Sound and Vibration*, Vol. 76, Number 3, 1981, pp 329-360.
3. Burgreen, D., Byrnes, J.J., and Benforado, D.M., 1958, "Vibration of Rods Induced by Water in Parallel Flow," *Transactions of the ASME*, **80**, pp. 991—1003.
4. Reavis, J.R., 1969, "Vibration correlation for maximum fuel-element displacement in parallel turbulent flow," *Nuclear Science and Engineering*, **38**, pp. 63-69.

5. Basile, D., Faure, J., and Ohlmer, E., 1968, “Experimental study on the vibrations of various fuel rod models in parallel flow,” *Engineering and Design*, **7**, pp17-534.

6. Saito, N., Miyano, H., and Furukawa, S., 1990, “Study on vibration response of pipes induced by internal flow,” *Pressure Vessels and Piping Conference*, ASME Pressure Vessels Piping Division Publication PVP, pp. 233-238.

7. Durant, C., Robert, G., Filippi, F., and Mattei, P., 2000, “Vibroacoustic response of a thin cylindrical shell excited by a turbulent internal flow: comparison between numerical prediction,” *Journal of Sound and Vibration*, **229**, pp. 1115-1155.

8. Durant, C., and Robert, G., 1998, “Vibroacoustic response of a pipe excited by a turbulent internal flow,” *Turbulence and Combustion*, **61**, pp. 55-69.

9. Brevart, B., and Fuller, C., 1993, “Effect of an internal flow on the distribution of vibration energy in an infinite fluid filled thin cylindrical elastic shell,” *Journal of Sound and Vibration*, **167**, pp. 149-163.

10. Kim, Y.K. and Kim, Y.H., 1996, “Three accelerometer method for the measurement of flow rate in a pipe,” *Journal of Acoustical Society of America*, **100**, pp. 717-726.

11. Pittard, M.T., Evans, R.P, Maynes, D., and Blotter, J.D., 2004, “Experimental and numerical investigation of turbulent flow induced vibration in fully developed flow,” *Review of Scientific Instruments*, **75**, pp. 2393-2401.

12. Evans, R.P., Blotter, J.D., Stephens, A.G., “Flow Rate Measurements Using Flow-Induced Pipe Vibration,” *Transactions of the ASME,* Vol. 126, March 2004, pp 280-285.

13. Caillaud, S., Gibert, R., Moussou, P., Cohen, J., Millet, F., “Effects on Pipe Vibrations of Cavitation in an Orifice and in Globe-Style Valves,” *Proceedings of Pressure Vessels and Piping Conference,* July, 2006.

14. Moussou, P., “An Attempt to Scale the Vibrations of Water Pipes,” *Transactions of the ASME,* Vol. 128, November 2006, pp 670-676.

15. Shurtz, T.P., *Analysis of Induced Vibrations in Fully-Developed Turbulent Pipe Flow Using a Coupled LES and FEA Approach,* Brigham Young University, Provo, UT, USA, Master’s Thesis, 2009.